IS-T-538

ELASTIC PROPERTIES OF POLYCRYSTALLINE Gd_2O_3

M. S. Thesis Submitted to Iowa State University,
August, 1972

J. A. Haglund

Ames Laboratory, USAEC
Iowa State University
Ames, Iowa 50010

Date of Manuscript: August, 1972

PREPARED FOR THE U. S. ATOMIC ENERGY COMMISSION
DIVISION OF RESEARCH UNDER CONTRACT NO. W-7405-eng-82

DISCLAIMER

Available from: National Technical Information Service
Department A
Springfield, VA 22151

Price: Microfiche $0.95

Elastic properties of polycrystalline Gd_2O_3

by

John August Haglund

A Thesis Submitted to the
Graduate Faculty in Partial Fulfillment of
The Requirements for the Degree of
MASTER OF SCIENCE

Major: Ceramic Engineering

Approved:

Orville Hunter
In Charge of Major Work

For the Major Department

For the Graduate College

Iowa State University
Ames, Iowa

1972

TABLE OF CONTENTS

Abstract

Elastic properties of polycrystalline Gd_2O_3

John August Haglund

A resonant frequency technique was used to determine the effect that temperature and porosity have on the elastic properties of gadolinia, while the temperature dependence of thermal diffusivity was investigated by a flash method.

Young's modulus, shear modulus, and Poisson's ratio were studied from 2.48% to 36.78% porosity to yield porosity dependence curves, with the extrapolated 0% porosity values enabling the calculation of the Debye temperature. Selected specimens were chosen to be analyzed from room temperature to 1352°C to determine curves for the temperature dependence of Young's modulus, shear modulus, Poisson's ratio, bulk modulus, and the first (γ) and second (δ) Grüneisen constants.

Thermal diffusivity was measured and graphed over the temperature range 151-1347°C and the thermal conductivity was calculated from these results.

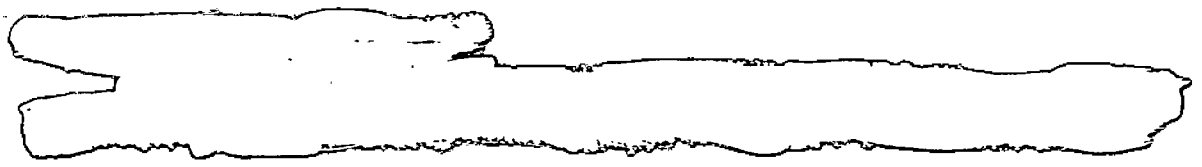

INTRODUCTION

Gadolinium oxide (Gd_2O_3) has a great potential in the field of nucleonics due to its enormous thermal neutron absorption cross section of over 40,000 barns and its refractory nature. Gadolinium oxide can be homogeneously mixed with UO_2 as a "burnable poison" for use in nuclear fuels, or mixed with alumina and shaped into pea-size spheres or thumb-size cylinders to be quickly introduced into a reactor to shut it down in an emergency, thereby acting as an "atomic fire extinguisher" (1). Metallurgists have also learned how to incorporate gadolinium oxide into austenitic stainless steels that can be hot worked (2) for use in nuclear control applications.

For design considerations the elastic properties of gadolinium oxide must be known at not only room temperature, but also at elevated temperatures. Gadolinium oxide is often porous as a result of the sintering process used in fabrication, and thus the variation in elasticity with porosity is also of prime importance. Another property which is used in design considerations is thermal diffusivity. Since thermal shock failure occurs under transient temperature conditions thermal diffusivity must be taken into account. It is generally assumed that thermal shock resistance is directly proportional to thermal diffusivity and therefore is of great interest.

This study uses a resonant frequency technique to measure the variations of Young's modulus, shear modulus, Poisson's ratio, bulk modulus, and the first (γ) and second (δ) Grüneisen constants in monoclinic Gd_2O_3 as a function of temperature and specimen porosity. The Debye temperature is also determined by extrapolating the data to 0% porosity. An analysis is made of the thermal diffusivity and conductivity as a function of temperature.

LITERATURE REVIEW

Elasticity Theory

The first reported work (3,4,5) utilizing a resonant technique for the determination of the elastic moduli of materials was associated with ferromagnetic or ferromagnetic-impregnated materials to facilitate the electrical observation of the vibrations. A method of supporting nearly any rigid sample by suspending it with threads near the nodal points and observing it in flexural resonance was later described by Forster (6). A detailed description of the experimental technique has been given by Spinner and Tefft (7) and, more recently, by Marlowe (8).

The effects of shearing forces on adjacent cross-sectional elements of a vibrating bar were first analyzed by Timoshenko (9,10) in 1921. Since that time there have been several studies (11,12,13) concerning the effect of shape and elasticity on the resonant flexural frequency of a vibrating bar. Pickett (14) has given a set of equations for the computation of correction factors to account for the effects of rotary inertia and shear.

The equation (7) for a rectangular prism relating the shear modulus to the fundamental resonant frequency of torsional vibration is

$$G = \frac{4L\ R\ m\ f_t^{\,2}}{A} \qquad (1)$$

where G is the shear modulus,

L is the length of the specimen,

m is the mass of the specimen,

f_t is the fundamental torsional frequency,

A is the cross-sectional area,

and R is a shape factor given by

$$R = \frac{a/b + b/a}{4(a/b) - 2.52(a/b)^2 + 0.21(a/b)^6}$$

where a is the length of the short side

and b is the length of the long side of the cross-section.

Spinner et al. (7,15) have studied Pickett's (14) equations relating Young's modulus to the fundamental resonant frequency of flexural vibration for a prism with rectangular cross-section and have developed the equation

$$E = 0.94645 \frac{S\, m\, f_f^2}{c} \qquad (2)$$

where E is the Young's modulus,

m is the mass of the specimen,

f_f is the fundamental flexural frequency,

c is the cross-sectional dimension perpendicular to the direction of vibration,

and S is a shape factor given by

$$S = [1 + 6.5850(1+0.0752\mu+0.8109\mu^2)(d/L)^2 - \frac{8.340(1+0.2023\mu+2.173\mu^2)(d/L)^4}{1 + 6.338(1+0.14081\mu+1.536\mu^2)(d/L)^2} - 0.86806(d/L)^4](d/L)^{-3}$$

where d is the cross-sectional dimension parallel to the direction of vibration,

L is the length of the specimen,

and μ is Poisson's ratio.

Since Poisson's ratio would not be known, a value would have to be assumed and an approximate Young's modulus value calculated utilizing Equation 2. The shear modulus and the Young's modulus approximation could then be used with the relation

$$\mu = \frac{E}{2G} - 1 \qquad (3)$$

where all terms are previously defined, to calculate a Poisson's ratio. A comparison of the calculated and the assumed values of μ could then be made to determine the accuracy of the assumption; if too much discrepancy existed, another approximate Young's modulus could be calculated using the newest value of μ. This procedure could be repeated until the desired degree of correlation existed.

The role that porosity plays in affecting the mechanical properties of materials has been a subject of prime interest (16,17,18,19). The experimental work done concerning the porosity dependence of elastic properties has produced several relations.

Aluminum oxide has been studied by Coble and Kingery (20) at porosity levels up to about fifty percent. Their results showed that aluminum oxide closely approximates the theoretical relationships derived by Mackenzie (17), which can be written

as

$$\frac{G}{G_o} = 1 - \frac{15(1-\mu_o)}{(7-5\mu_o)} P - DP^2 \qquad (4)$$

and when combined with Equation 3

$$\frac{E}{E_o} = \frac{\mu+1}{\mu_o+1} \left[1 - \frac{15(1-\mu_o)}{(7-5\mu_o)} P - DP^2\right] \qquad (5)$$

where G is the shear modulus,

G_o is the shear modulus at 0% porosity,

E is the Young's modulus,

E_o is the Young's modulus at 0% porosity,

μ is Poisson's ratio,

μ_o is Poisson's ratio at 0% porosity,

P is the volume fraction porosity,

and D is a constant.

When calculating the value of D it is necessary to assume a value for μ_o and set a boundary condition. Coble and Kingery (20) assumed that G = 0 when P = 1. Marlowe and Wilder (21), along with Manning et al. (22), have stated that the boundary condition should be G = 0 at P = 0.4764 because 0.4764 is the volume fraction porosity for primitive cubic packing of uniform sized spherical particles. It would then be the minimum density that could exist for a material of that type and any increase of porosity beyond that point would destroy the continuity of the solid.

Spriggs (23) proposed that the relationship between Young's modulus and porosity was of the same form as Duck-

worth's (24) commentary on Ryshkewitch's (25) study of the compressive strength of refractory ceramic materials, i.e.

$$E/E_o = e^{-BP} \tag{6}$$

where E, E_o, and P have been previously defined,

e is the Naperian constant,

and B is an empirical constant.

Spriggs and Brissette (26) went on to extend the semi-logarithmic relationship to the shear modulus, giving the relation

$$G/G_o = e^{-B'P} \tag{7}$$

where B' is an empirical constant.

It was noted by Hasselman (27) that at no realistic value of P would Equations 6 or 7 yield a value of zero for the elastic moduli. Because of this inability to satisfy the boundary conditions and based on the theoretical relationship by Hashin (19) he proposed an expression to explain the relationship between the elastic moduli and porosity of the form

$$M/M_o = 1 - \frac{cP}{1+(c-1)P} \tag{8}$$

where M is Young's or shear modulus at temperature T,

M_o is Young's or shear modulus at room temperature,

c is a constant,

and P is previously defined.

A simple linear relation, advocated by Fryxell and Chandler (28), has been proposed to have the form

$$M = M_o(1-AP) \tag{9}$$

where M, M_o and P have been previously defined and A is a constant.

When concerned with the effect that a change in temperature has on both Young's and shear moduli it is necessary to consider thermal expansion of the sample in Equations 1 and 2. A complete recalculation of each equation is not necessary, however, and the moduli at a given temperature can be determined from room temperature values by the relation

$$M_T = M_o \frac{f_T^2}{f_o^2} \frac{1}{(1+\alpha\Delta T)} \tag{10}$$

where M_T is Young's or shear modulus at temperature T,

M_o is Young's or shear modulus at room temperature,

f_T is the fundamental flexural frequency at temperature T when M_o is Young's modulus or the fundamental torsional frequency at temperature T when M_o is shear modulus,

f_o is the fundamental flexural frequency at room temperature when M_o is Young's modulus or the fundamental torsional frequency at room temperature when M_o is shear modulus,

α is the coefficient of linear thermal expansion,

and ΔT is the difference between elevated temperature T and room temperature.

Once the values of both Young's and shear moduli have been calculated at the elevated temperature it is a simple task to calculate Poisson's ratio at that temperature through

the use of Equation 3.

Characterization of the temperature dependence of the moduli seems to yield an approximately linear dependence for many crystalline solids and Wachtman et al. (29) have proposed a relation of the form

$$M_T = M_{|0|} - kT \exp(-T_o/T) \qquad (11)$$

where M_T is either Young's or shear modulus at temperature T,

$M_{|0|}$ is either Young's or shear modulus at absolute zero,

T is the elevated absolute temperature,

T_o is an absolute temperature constant,

and k is a constant.

This approaches a linear relation as T_o approaches zero.

Once Young's and shear moduli have been thoroughly described, other elastic properties can be calculated for isotropic materials. The adiabatic bulk modulus (30) can be calculated from Young's and shear moduli by the equation

$$B_T = E_T G_T / 3(3G_T - E_T) \qquad (12)$$

where B_T, E_T, and G_T are, respectively, bulk modulus, Young's modulus, and shear modulus at temperature T.

The Debye temperature, an important parameter of solids, can be defined (31) as

$$\theta = \frac{h}{k} \left[\frac{3qN\rho}{4\pi M} \right]^{1/3} \nu_m \qquad (13)$$

where θ is the Debye temperature,

h is Planck's constant,

k is Boltzmann's constant,

q is the number of atoms in the molecular formula,

N is Avogadro's number,

ρ is the density,

M is the molecular weight,

and ν_m is the mean sound velocity.

For isotropic materials it has been shown (32,33) that

$$\nu_m = \left[\frac{1}{3}\left(\frac{2}{\nu_s^3} + \frac{1}{\nu_\ell^3} \right)\right]^{-1/3}$$

where ν_s and ν_ℓ are the shear and longitudinal sound velocities having the forms

$$\nu_s = \left(\frac{G}{\rho} \right)^{1/2}$$

$$\nu_\ell = \left[\frac{G(4G-E)}{\rho(3G-E)}\right]^{1/2}$$

where ρ is density,

G is shear modulus,

and E is Young's modulus.

With a knowledge of the specific heat, the coefficient of linear thermal expansion, and the bulk modulus, both the first (γ) and second (δ) Grüneisen constants can be calculated (29,34) using the following relations

$$\gamma = \frac{3\alpha V_T B_T}{C_p} \qquad (14)$$

$$\delta = \frac{1}{3\alpha B_T} \frac{dB_T}{dT} \qquad (15)$$

where α is the coefficient of linear thermal expansion,

V_T is the molar volume at temperature T,

B_T is the bulk modulus at temperature T,

C_p is the specific heat at constant pressure,

and dB_T/dT is the slope of the bulk modulus versus temperature curve.

The dynamic resonance principle for determining elastic properties has been applied to several rare-earth oxides. Yttrium oxide, dysprosium oxide, erbium oxide, and holmium oxide (21,22,30,35,36) have been studied with respect to the temperature and porosity dependence of Young's modulus, shear modulus, bulk modulus, Poisson's ratio, Debye temperature, and the first (γ) and second (δ) Grüneisen constants. Others, such as thorium oxide (37,38), ytterbium oxide (39), thulium oxide, and lutetium oxide (40), have been only partly characterized.

Thermal Diffusivity Theory

Thermal diffusivity is a measure of how rapidly a thermal disturbance will travel through a sample and has been defined (41) as

$$\alpha_T = \lambda / \rho C_p \qquad (16)$$

where α_T is thermal diffusivity,

λ is thermal conductivity,

ρ is density,

and C_p is the specific heat at constant pressure.

In 1961 Parker et al. (42) proposed a technique known as the flash method for measuring thermal diffusivity. This method utilizes a small, thermally insulated disk that has one face exposed to a short pulse of energy. Thermal diffusivity is determined by monitoring the time-temperature history of the back face after the thermal disturbance.

It has been shown (42,43,44) that the theoretical thermal reaction of the back face to a short pulse of energy supplied to the front of a uniformly thick sample is of the form

$$V = 1 + 2 \sum_{n=1}^{\infty} (-1)^n \exp(-n^2 W)$$

having $V = T(L,t)/T_M$

and $$W = \pi^2 \alpha_T t / L^2 \qquad (17)$$

where $T(L,t)$ is the temperature of the rear face of a sample of thickness L after time t,

T_M is the maximum rear face temperature reached,

and α_T is thermal diffusivity.

This theoretical curve is plotted in Figure 1.

Parker et al. (42) noted that in theory when $V = 0.5$, $W = 1.38$. Using this arbitrary, but much used, point in Equation 17 yields

$$\alpha_T = 1.38 L^2 / \pi^2 t_{1/2} \qquad (18)$$

where $t_{1/2}$ is the time required for the temperature of the rear face of the specimen to reach half its maximum value.

The flash method of determining thermal diffusivity has

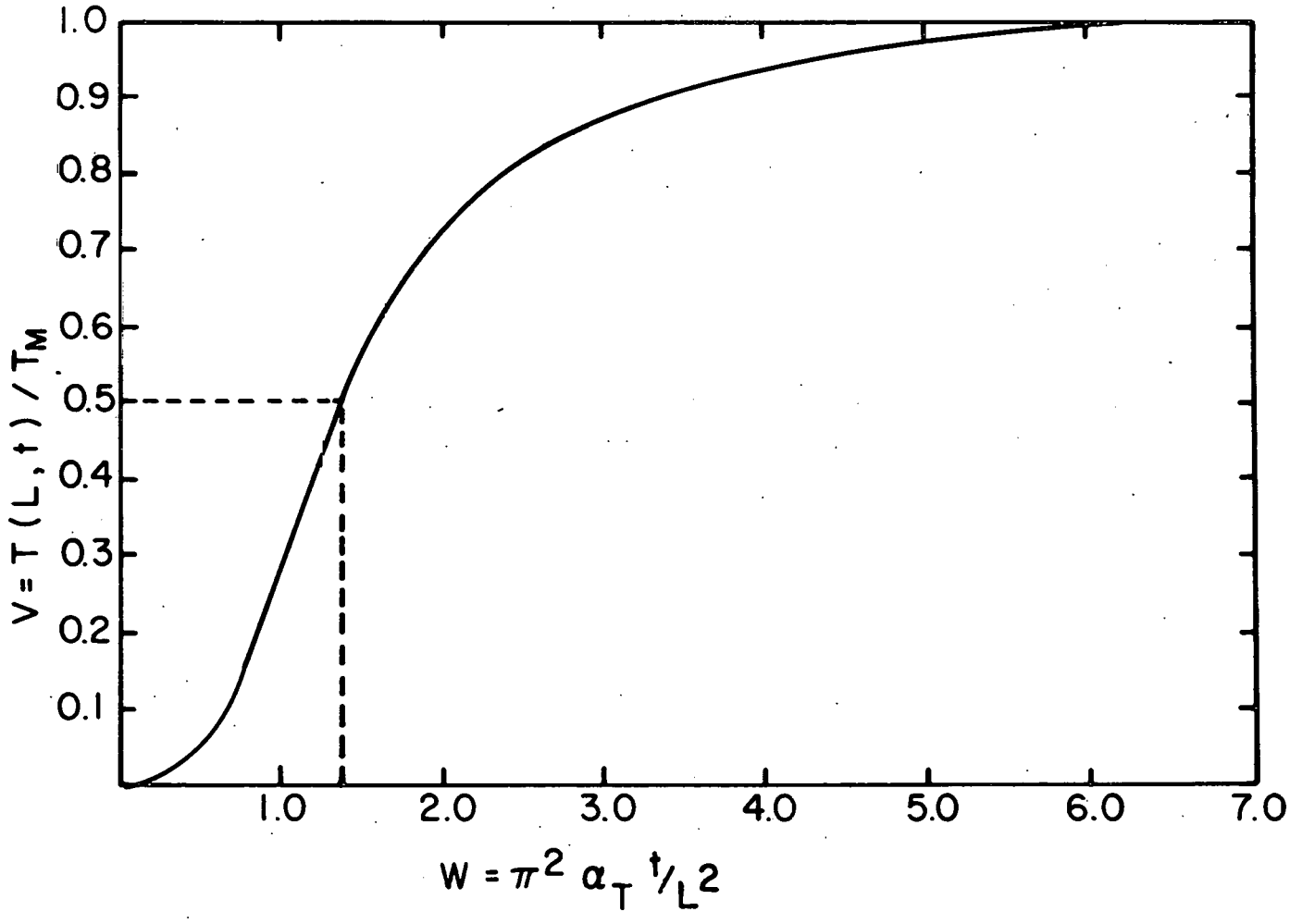

Figure 1. Theoretical thermal history of rear face.

received a great deal of consideration in the literature (44, 45,46,47). A pulsed ruby laser was used by Deem and Wood (48) in 1962 as the energy source in a study of the thermal diffusivity of stainless steel and graphite. Several authors (49,50,51,52) have used this method to evaluate the thermal diffusivity of radioactive and reactor materials, while Moser and Kruger (53), in a study of UC, UP, and US, were the first to correct for porosity and obtain heat capacity data by this method. Zhuze et al. (54) have investigated the thermal diffusivities of the single crystal rare-earth oxides Y_2O_3, Er_2O_3, Lu_2O_3, and Sm_2O_3.

Several relations have been found to express the temperature dependence of thermal diffusivity. In his work with ATJ-S graphite Morrison (55) found that the best relation was of the form

$$\alpha_T = A + \frac{B}{T} + \frac{C}{T^2} \qquad (19)$$

where α_T is thermal diffusivity,

T is temperature,

and A, B, and C are constants.

Branscomb and Hunter (44) found a similar relation

$$\alpha_T = A + \frac{B}{T} \qquad (20)$$

to be representative of their work with TiB_2, ZrB_2, and HfB_2. Nakata et al. (56) observed that the best fit for the temperature dependence of thermal diffusivity for some zirconium-

uranium hydrides was of the form

$$\alpha_T = A + BT + CT^2 \tag{21}$$

while for others it was

$$\alpha_T = A + BT + CT^2 + DT^3 \tag{22}$$

where D is a constant. Weeks et al. (57) also found that Equation 22 was the optimal fit for their SNAP fuel data.

Thermal conductivity can be easily calculated from Equation 16 once the thermal diffusivity is known, since heat capacity data are usually available. This is a very desirable way to determine thermal conductivity, especially at high temperatures, since it requires only simple measurements of length and time rather than the inherently less accurate measurements of temperature gradients and heat fluxes required for standard thermal conductivity determinations.

EXPERIMENTAL PROCEDURE

Specimen Preparation and Characterization

The gadolinium oxide was provided by Ames Laboratory as clinker from the calcined oxalate and was reduced to a powder by hand grinding with a Diamonite mortar and pestle. It was found to have a purity of better than 99.75%; a semiquantitative analysis of the powder was performed by the Ames Laboratory Spectrographic Group and the results appear in Table I.

Table I. Spectrographic analysis of impurities

Element	Concentration (ppm)	Element	Concentration (ppm)
Al	<10	Mg	<20
Ca	<10	Nd	100
Cr	<10	Ni	<20
Cu	<20	Si	<20
Dy	<50	Sm	<100
Eu	<100	Ta	<200
Fe	60	Th	<500
Gd	constituent	W	<500
Ho	<200	Y	<500

The elastic property measurements utilized prismatic bars made by first recalcining the material at 740°C for 40 minutes and then mechanically pressing it in a steel, double-action die at 3000 psi followed by isostatic pressing at 30,000 psi. Sintering was accomplished by placing the bars on zirconia setters in a graphite-susceptor induction furnace and firing them in an air atmosphere at a variety of temperatures from 1695°C to 1950°C. They were then fired at 1200°C

under an air atmosphere in an electric resistance furnace to eliminate the graphite contamination acquired during the sintering process.

X-ray measurements were made to confirm that the crystallographic form was monoclinic and analysis of the microstructure indicated that the average grain size after firing was approximately 13 microns.

A surface grinder was used to machine the specimen surfaces flat and parallel within 0.001 cm. The bulk densities were computed from the dimensions and masses of the specimens after drying them at 740°C. The volume fraction porosities of the sintered bars were calculated using the relation porosity = 1 - (measured density/theoretical density). The theoretical density of monoclinic gadolinium oxide was calculated to be 8.348 g/cm^3 based on the lattice parameters given by Stecura (58).

Appendix A gives the dimensions, density, and volume fraction porosity for each of the sintered specimens.

Fabrication of specimens for the thermal diffusivity measurements included the same preliminary preparation as used for the elastic property measurements, except that a 3/4 inch diameter cylindrical disk was produced rather than a rectangular bar. The specimens were fired under vacuum in a furnace using a tungsten mesh heating element at various temperatures in the range 1850-1980°C.

A surface grinder was used to machine the cylinder to a thickness of approximately 0.5 cm with ends flat and parallel to within 0.001 cm. The specimen configuration proposed by Branscomb (43,44) was adopted. This required that the whole cylinder be ground to a diameter of about 1.27 cm followed by a further reduction to a diameter of about 1.11 cm along two-thirds of the cylinder length. This procedure formed a lip on the cylinder end having a 3:1 ratio of cylinder length to lip thickness. The reason for this lip-type specimen was to form a light seal with the support system to avoid damaging the detector by directly exposing it to the laser beam. As a precaution against direct transmission of the laser beam through the specimen to the detector, each specimen was coated with a thin layer of colloidal platinum suspended in an organic base (Englehard No. 6082) to absorb the incident light.

Appendix B gives the densities, volume fraction porosities, and thicknesses of the specimens before application of the colloidal platinum.

Elasticity Measurements

The Forster (6) technique, which was mentioned earlier, was used to observe the sonic resonance of the specimens in this study.

A block diagram of the equipment is given in Figure 2. A sinusoidal electrical signal was produced by a wide range

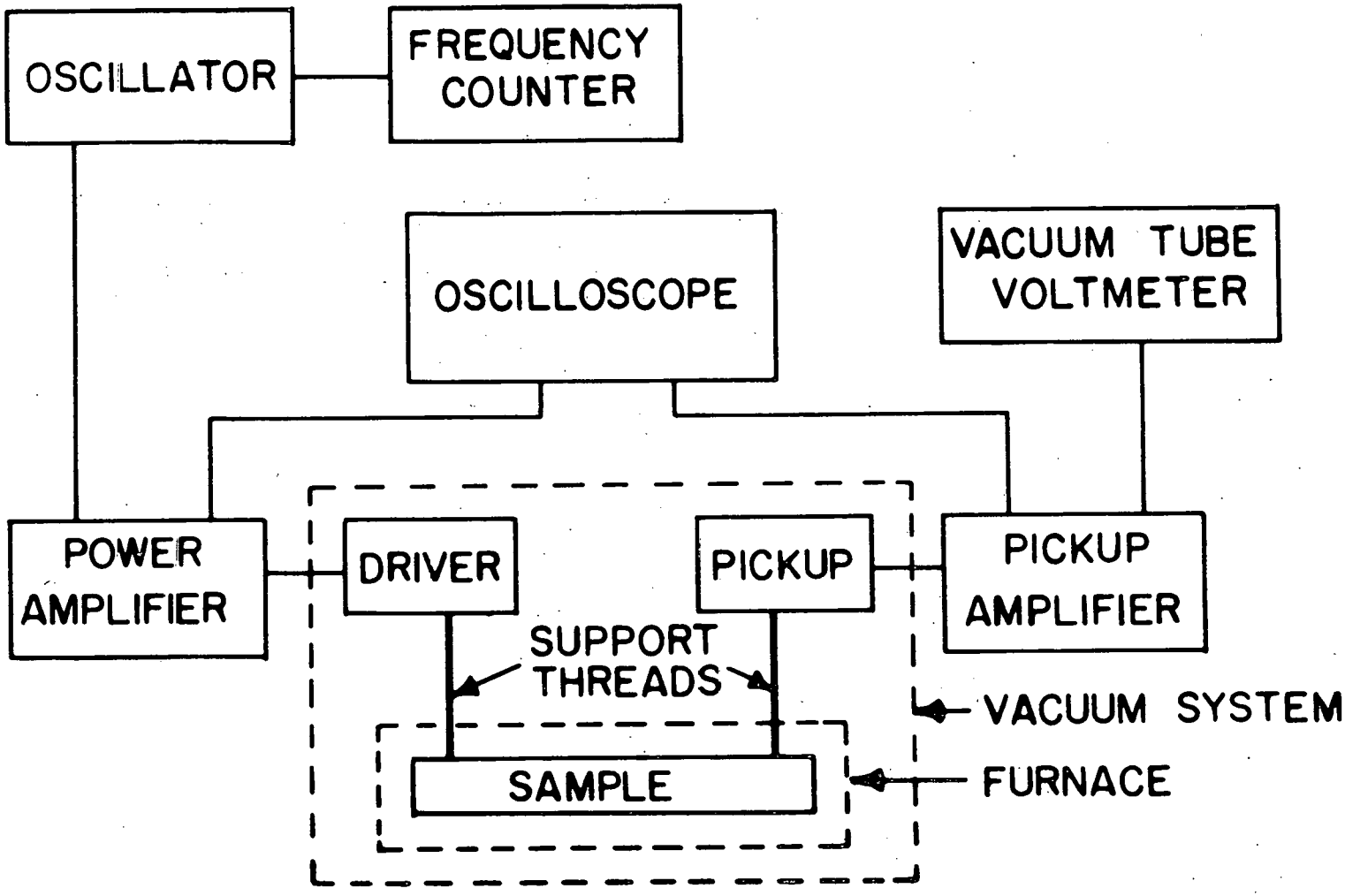

Figure 2. Block diagram of resonant frequency equipment.

(5 to 50,000 hertz) variable frequency oscillator (Hewlett-Packard model 200CD) that supplied a signal not only to a power amplifier (Heathkit model EA-3, 14 watts) for amplification and control, but also to an electronic frequency counter (Hewlett-Packard model 5223L) for exact monitoring of the input signal. The amplified signal was converted to mechanical vibration by the driver, a magnetic transcription cutting head (Astatic type M41-8).

The coupling of the signal from the driver to the pickup was accomplished by suspending the specimen between them. Cotton suspending threads were used for the room temperature work while carbon yarn (Hitco) was used for the high temperature readings.

A high-output piezoelectric phonograph cartridge (Astatic 62-1) was used to convert the mechanical vibration transmitted through the sample back to electrical impulses. A pickup amplifier (designed and built by Ames Laboratory Instrumentation Group) was used to amplify the signal before it was fed to a vacuum tube voltmeter (Hewlett-Packard model 400D), which was used to gauge the amplitude of the transmitted signal. As a visual aid in observing resonance of the sample an oscilloscope (Hewlett-Packard model 130 BR) was introduced into the system in such a way that the output of the power amplifier was applied to the horizontal plates of the scope while the output of the pickup amplifier was applied to the vertical plates.

The elevated temperature elasticity data were taken under vacuum at pressures less than $5x10^{-5}$ torr. The specimen was suspended in a manually-controlled carbon-rod resistance furnace, and the temperature was sensed by a Pt-Pt 10% Rh thermocouple having the measuring junction near the center of the specimen. Thermal equilibrium was ensured by monitoring the thermocouple output with a millivolt recorder. A more detailed description of the furnace and vacuum system can be found in the work by Marlowe (8).

The resonant frequency was determined approximately by varying the signal from the oscillator until the suspended specimen vibrated in resonance producing a Lissajous pattern on the oscilloscope. Further tuning of the oscillator to give maximum deflection on the vacuum tube voltmeter allowed the exact resonant frequency to be read on the frequency counter.

The type of resonant vibrational mode associated with each resonant frequency peak was determined by probing the specimen while vibrating. Three non-longitudinal, fundamental resonant vibrational modes can be associated with a rectangular prism (59) and are illustrated in Figure 3. The relative amplitudes of vibrational displacement are indicated by arrows and nodes are shown as dotted lines.

Only the torsional vibration and one type of flexural vibration are required for the calculation of the elastic moduli, but the other acts as a good check on the homogeneity and isotropy of the sample (7). The frequencies associated

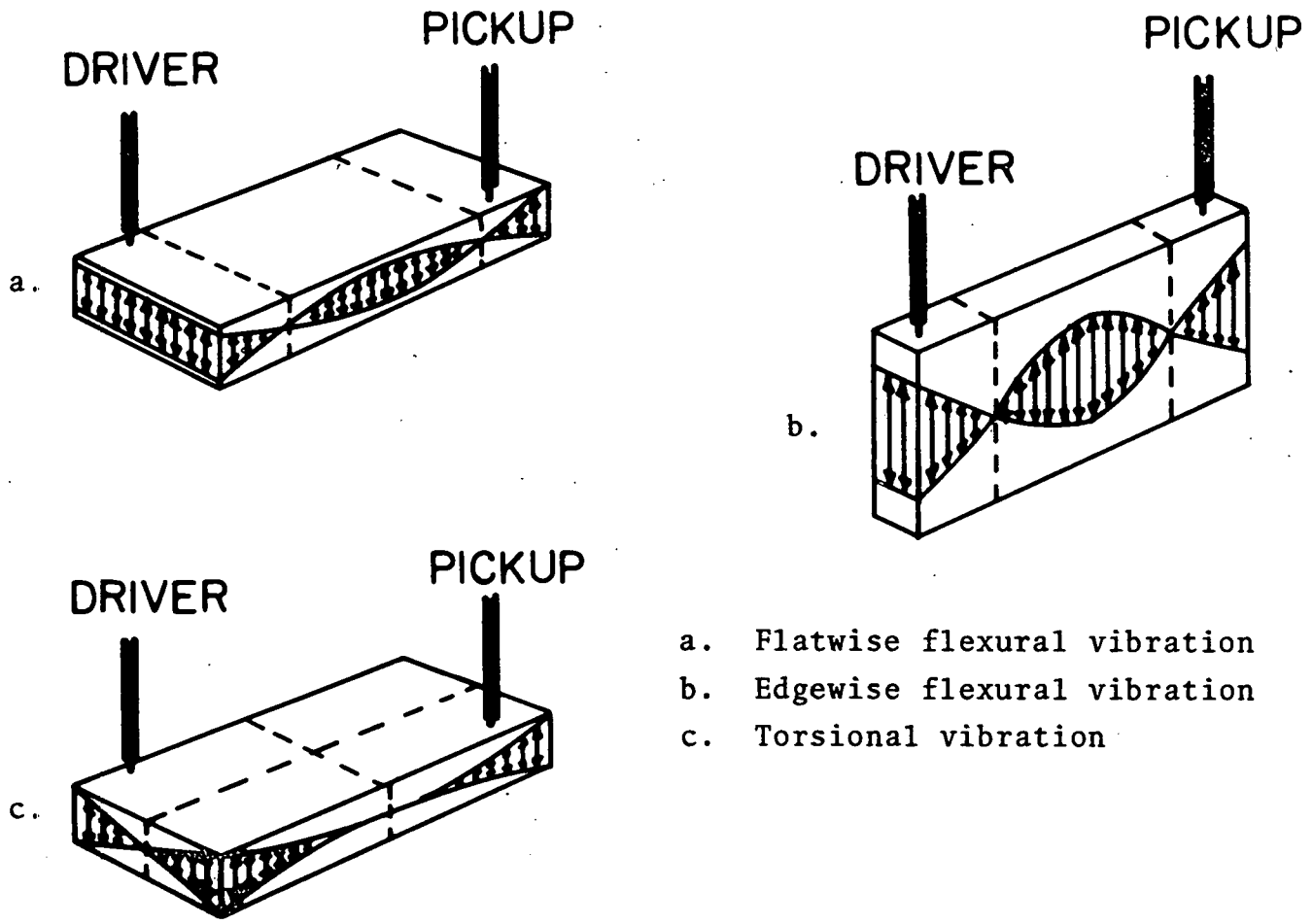

a. Flatwise flexural vibration
b. Edgewise flexural vibration
c. Torsional vibration

Figure 3. Fundamental modes of resonant vibration in rectangular prisms.

with the flatwise flexural and the torsional modes of vibration were measured, along with the physical dimensions and mass of the specimen.

Thermal Diffusivity Measurements

The flash method, as described earlier, requires a short pulse of energy to be absorbed by one face of a specimen while the thermal history of the opposite face is noted. The source of energy in this study was a water-cooled ruby laser (Korad model K-1) having a maximum energy rating of 25 joules with a 500 microsecond peak width.

The specimen was positioned in a vacuum furnace utilizing a tantalum heating element operating under a pressure of 7×10^{-5} torr. Temperature of the specimen was measured with a Pt-Pt 10% Rh thermocouple.

A front-surface mirror was used to direct the laser beam onto the front surface of the specimen. An optical detector in the form of a photovoltaic indium antimonide infrared detector (American Electronic Laboratories, Inc.) was used to monitor the temperature of the rear face of the specimen. The output of the detector was enhanced by an amplifier (designed and built by Ames Laboratory Instrumentation Group) before it was supplied to a recorder (Honeywell Visicorder model 906C) used to produce a time versus temperature plot.

A block diagram of the equipment is given in Figure 4 and a more detailed description is given in the work of

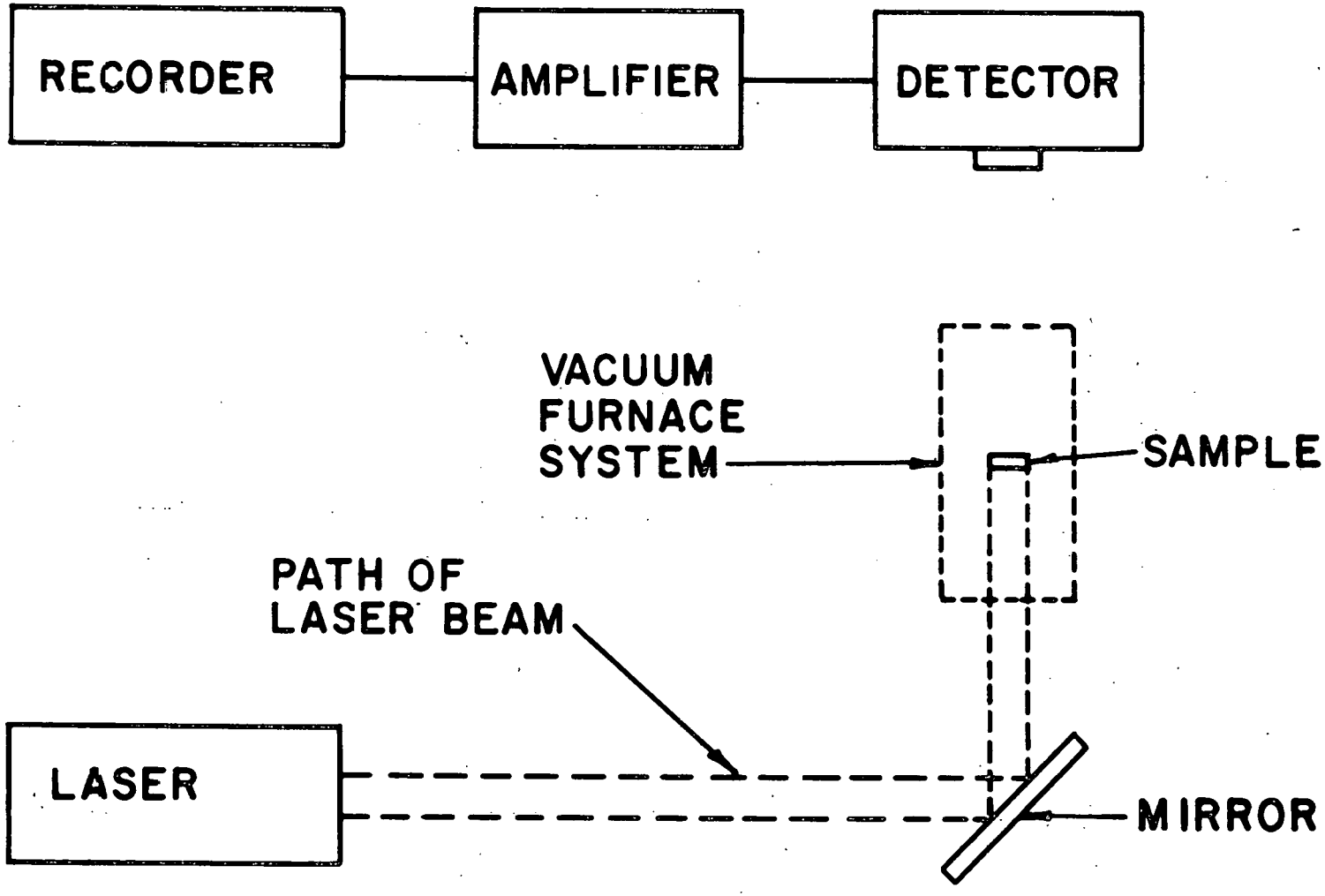

Figure 4. Block diagram of thermal diffusivity equipment.

Branscomb (43,44).

Alignment of the equipment was necessary before inserting the sample into the furnace to ensure that the most intense portion of the laser beam fell on the specimen. This was accomplished by reflecting an ordinary light beam off the front face of the ruby crystal. The front-surface mirror was then adjusted until the image of the end of the ruby, as observed by sighting down through the furnace tube, appeared to be centered within the tube.

Alignment of the detector unit was necessary after the specimen was placed in the furnace to ensure that it was recording the temperature of the rear face of the specimen. This was accomplished by heating the specimen to red heat and positioning the detector so that the recorder deflected a maximum amount.

The initial and maximum values of the rear face temperature were taken to be the middle of the band of noise on the recorder trace. Using the instant the laser flashed as time zero, the value $t_{1/2}$ was defined as the elapsed time for the rear face temperature to reach half its maximum value.

RESULTS AND DISCUSSION

Room Temperature Elastic Properties

The shear and Young's moduli of the specimens at room temperature were calculated from their masses, dimensions, and fundamental flexural and torsional resonant frequencies using Equations 1 and 2. These calculated values were then used in Equation 3 to yield Poisson's ratio. This information is tabulated in Appendix A, and the calculated elastic properties are plotted as a function of porosity in Figure 5.

A least-squares technique was used to fit the Young's and shear moduli data to Equations 4-9, which represent several of the theories and empirical relationships that have been successful in describing the porosity dependence of elastic moduli; the resulting curves are superimposed on the data points of Figure 5. The expressions best describing the data were taken to be those which provided the smallest standard error of estimate of the fit and, in both cases, were found to be linear of the form

$$E = 1502.6(1-1.7573P) \tag{23}$$

and

$$G = 588.5(1-1.7543P) \tag{24}$$

respectively for Young's and shear moduli.

Figure 6 shows the relative Young's modulus (E/E_o) and shear modulus (G/G_o) versus porosity for gadolinia, and indicates how they compare to other rare-earth oxides studied by

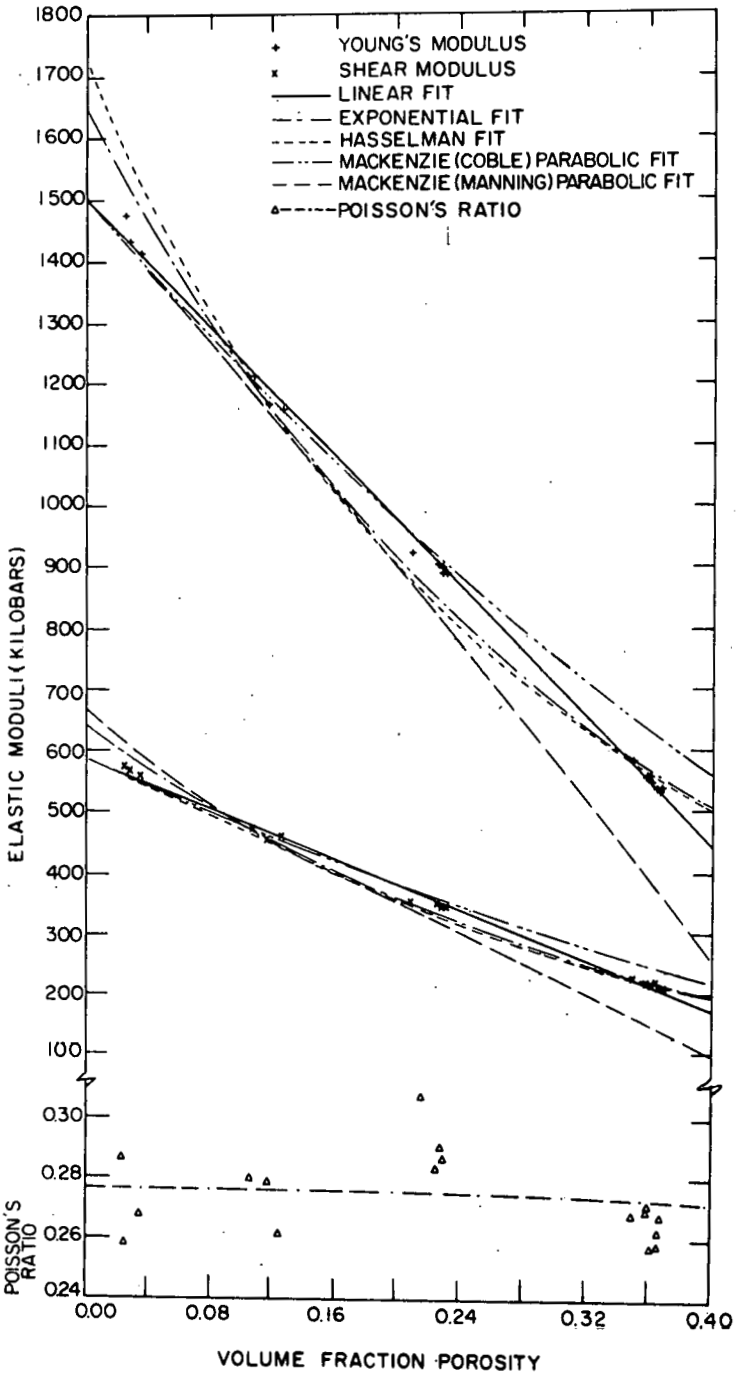

Figure 5. Room temperature Young's modulus, shear modulus, and Poisson's ratio versus volume fraction porosity.

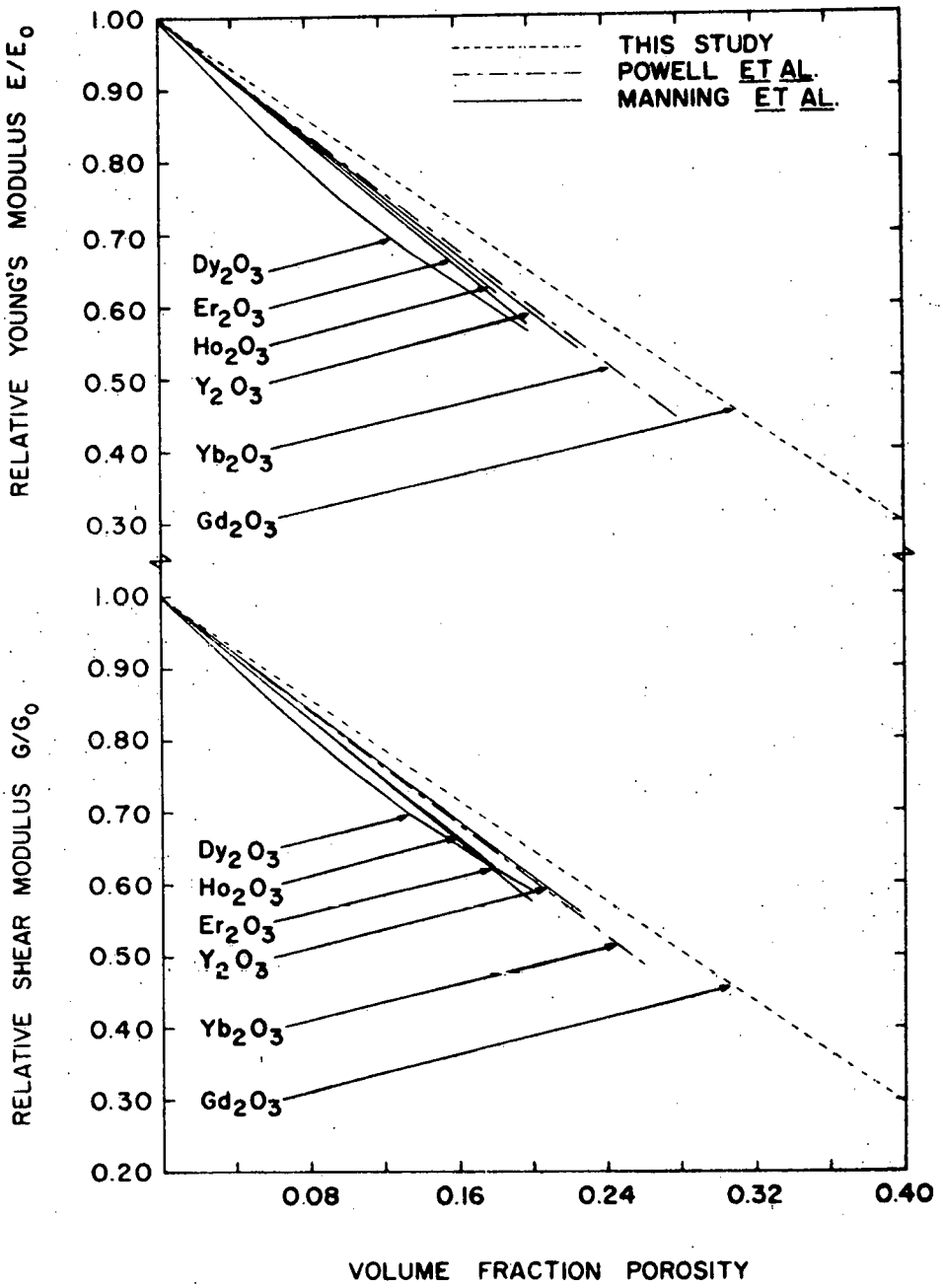

Figure 6. Relative Young's and shear moduli versus volume fraction porosity when related to past work.

Manning et al. (22) and Powell et al. (39). In all cases, the values obtained for Gd_2O_3 were larger than those obtained for the other rare earths. A possible explanation of this is that Gd_2O_3 possesses a different crystallographic structure than the other oxides. All the rare-earth oxides cited possess cubic structure, while Gd_2O_3 is monoclinic.

The best fits for the Young's and shear moduli data, Equations 23 and 24, were substituted into Equation 3 to give the resultant curve for the porosity dependence of Poisson's ratio. This method gave

$$\mu = \frac{0.2766 - 0.4892P}{1 - 1.754P} \qquad (25)$$

as the representation of the porosity dependence of Poisson's ratio and is shown in Figure 5. It is not surprising that there is more scatter about the calculated curve for Poisson's ratio than in the independently measured Young's and shear moduli from which Poisson's ratio was calculated (37).

A Debye temperature of 362°K was calculated from the room temperature elastic moduli data. This was accomplished by using the 0% porosity values of Young's and shear moduli in Equation 13.

Elevated Temperature Elastic Properties

Equation 10 was used to calculate the Young's and shear moduli at elevated temperatures; the thermal expansion information was taken from the work of Stacy (60). Poisson's ratio

was calculated from Equation 3 while Equation 12 was used to calculate bulk modulus. These values are tabulated in Appendix A and are plotted in Figure 7.

The Young's and shear moduli data were fitted to Equation 11; the resultant relations are shown in Table II and are plotted in Figure 7.

Table II. Equations for temperature dependence of Young's and shear moduli of the form $M_T = M_{|o|} - kT \exp(-T_o/T)$

Modulus	Volume fraction porosity	$M_{\|o\|}$ (kilobars)	k ($\frac{\text{kilobars}}{°K}$)	T_o (°K)
Young's	0.0347	1429.9	0.1792	266
Young's	0.2297	929.9	0.1507	0
Young's	0.3660	563.0	0.0948	0
Shear	0.0347	565.5	0.0698	216
Shear	0.2297	349.2	0.0586	208
Shear	0.3660	222.8	0.0377	0

The failure of the plot of moduli versus temperature to show a rapid drop off at some elevated temperature, as is observed in other polycrystalline materials (61), may be taken as an indication of the absence of grain boundary slippage (62, 63) in the temperature range studied.

As can be seen from the values of k in Table II, the temperature dependence of both Young's and shear moduli increase with increasing specimen density. This trend has also been observed by Spinner et al. (38) in his work with ThO_2.

The Poisson's ratio equations, shown in Table III, were

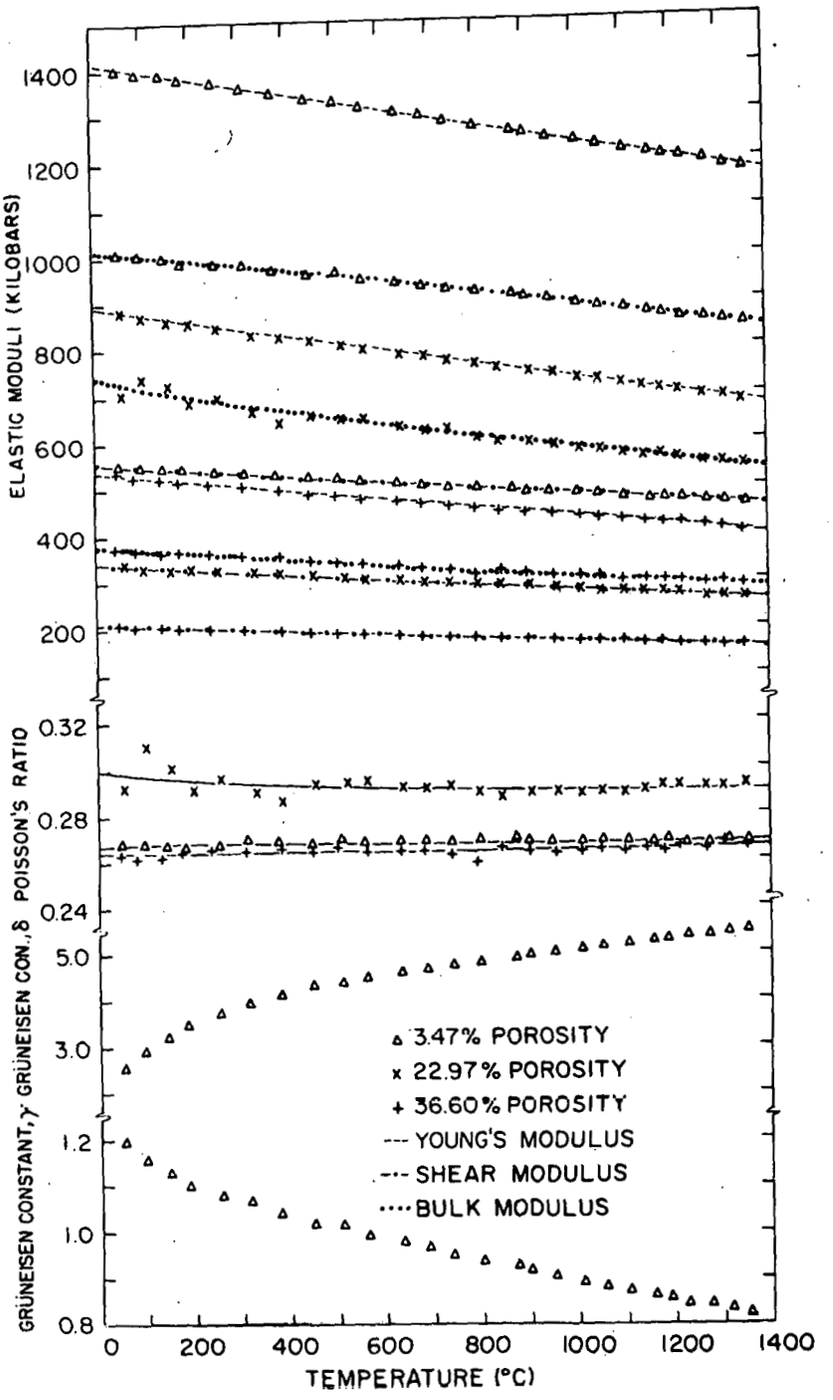

Figure 7. Elevated temperature Young's modulus, shear modulus, bulk modulus, Poisson's ratio, and Grüneisen constants versus temperature.

Table III. Equations for temperature dependence of Poisson's ratio of the form

$$\mu = \frac{A - BT \exp(-X/T) + CT \exp(-Y/T)}{1 - DT \exp(-Y/T)}$$

Volume fraction porosity	A	B ($\times 10^{-4}$) ($^\circ K^{-1}$)	C ($\times 10^{-4}$) ($^\circ K^{-1}$)	D ($\times 10^{-4}$) ($^\circ K^{-1}$)	X ($^\circ K$)	Y ($^\circ K$)
0.0347	0.2643	1.584	1.234	1.234	266	216
0.2297	0.3316	2.159	1.678	1.678	0	208
0.3660	0.2638	0.4377	0.000	1.691	0	0

calculated as before by using Equation 3 and the best fits for the elastic moduli data (Table II) rather than by forcing a least-squares fit to the individual Poisson's ratio data points.

The equations in Table II were also used to calculate the temperature dependence equations for the bulk modulus data by utilizing Equation 12. The results are given in Table IV.

The first (γ) and second (δ) Grüneisen constants were calculated for the densest specimen by using Equations 14 and 15. The work of Pankratz *et al.* (64) yielded values of C_p while the molar volume at temperature T was determined by the relation

$$V_T = \frac{\left(\frac{MW}{\rho_o}\right)(1+3\alpha\Delta T)}{(1-VFP)} \qquad (26)$$

Table IV. Equations for temperature dependence of bulk modulus of the form

$$B_T = \frac{A - BT\exp(-X/T) - CT\exp(-Y/T) + DT^2\exp(-Z/T)}{1 - ET\exp(-Y/T) + FT\exp(-X/T)}$$

Volume fraction porosity	A (kbars)	B ($\frac{kbars}{°K}$)	C ($\frac{kbars}{°K}$)	D ($\times 10^{-4}$) ($\frac{kbars}{°K^2}$)	E ($\times 10^{-3}$) ($°K^{-1}$)	F ($\times 10^{-3}$) ($°K^{-1}$)	X (°K)	Y (°K)	Z (°K)
0.0347	1011	0.1270	0.1247	0.1563	0.7850	0.6721	266	216	482
0.2297	921	0.1492	0.1542	0.2500	1.495	1.282	0	208	208
0.3660	397	0.1341	0.0000	0.1131	0.1726	0.0000	0	0	0

where V_T is molar volume at temperature T,

MW is molecular weight,

ρ_o is room temperature theoretical density,

α is coefficient of linear thermal expansion,

ΔT is the difference between temperature T and room temperature,

and VFP is the volume fraction porosity.

The computed values of the Grüneisen constants are plotted in Figure 7. These values agree favorably with the rare-earth oxide work of Manning and Hunter (30), but are more temperature dependent.

Thermal Diffusivity and Thermal Conductivity

The temperature dependence of thermal diffusivity was determined by Equation 18 with the thickness L being corrected for thermal expansion by the expression

$$L = L_o(1+\alpha\Delta T) \tag{27}$$

where L is the thickness at temperature T,

L_o is the room temperature thickness,

α is the coefficient of linear thermal expansion,

and ΔT is the difference between temperature T and room temperature.

A data point was taken as the average of three readings at each temperature. Values of the temperature, thickness, time, and thermal diffusivity are tabulated in Appendix B, while the values of thermal diffusivity are plotted in Figure 8.

The best expression for the data at each porosity was

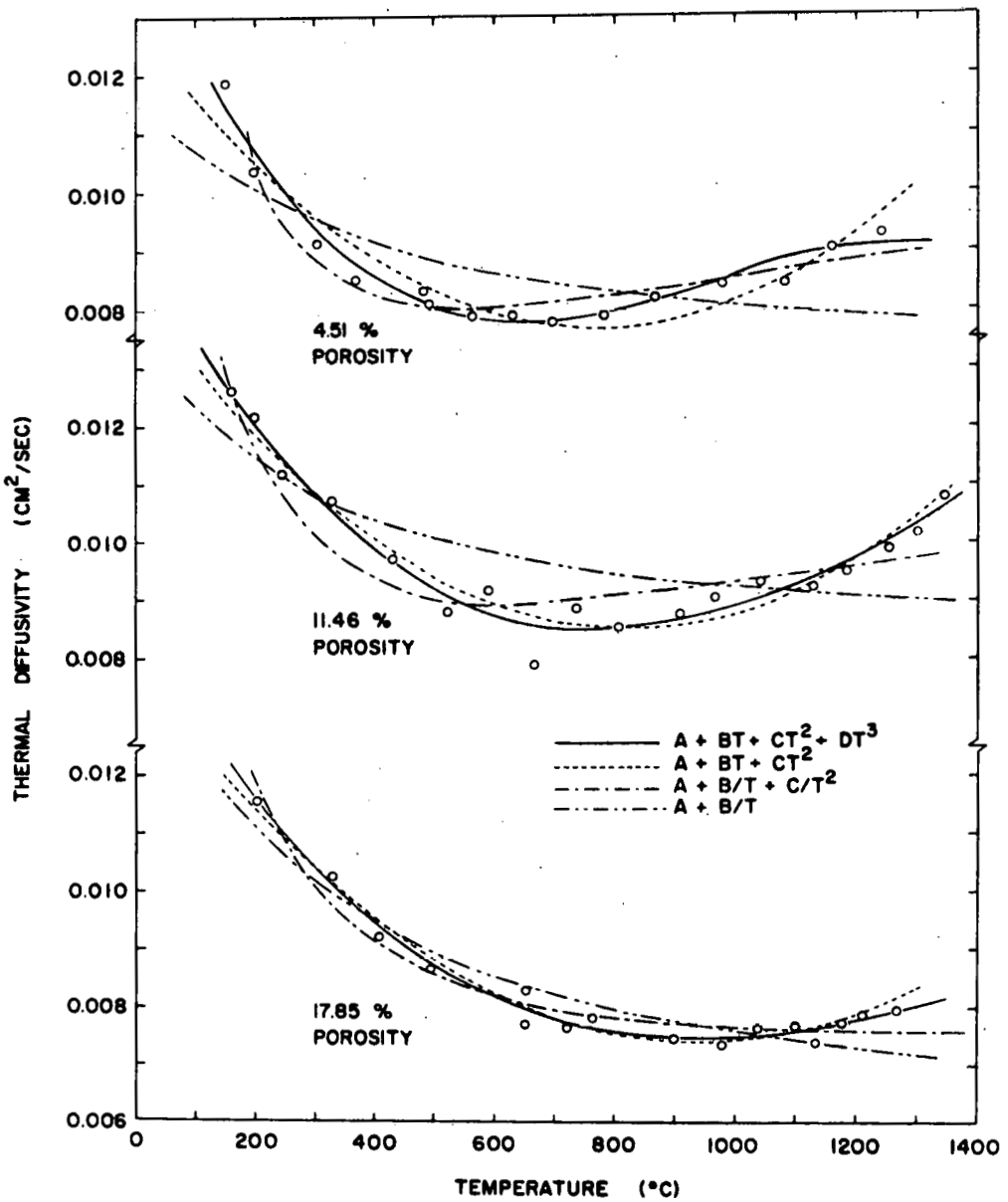

Figure 8. Thermal diffusivity versus temperature.

determined by first fitting them to Equations 19-22 by a least-squares method and selecting the one with the smallest standard error of estimate. In all cases a third order polynomial as a function of T in degrees Kelvin was the best fit, as is indicated in Table V and plotted in Figure 8.

Table V. Equations for the temperature dependence of thermal diffusivity of the form $A - BT + CT^2 - DT^3$

Volume fraction porosity	A ($\times 10^{-2}$) ($\frac{cm^2}{sec}$)	B ($\times 10^{-5}$) ($\frac{cm^2}{sec\text{-}°K}$)	C ($\times 10^{-8}$) ($\frac{cm^2}{sec\text{-}°K^2}$)	D ($\times 10^{-12}$) ($\frac{cm^2}{sec\text{-}°K^3}$)
0.0451	2.383	4.301	3.677	9.755
0.1146	2.268	3.204	2.239	4.473
0.1785	2.108	2.766	1.780	3.495

It was noted that the thermal diffusivity of Gd_2O_3 tended to increase above some elevated temperature. This has been observed in other materials (65,66) and has been explained by Flynn (67) as being due to radiation heat transfer within material porosity.

Figure 9 compares the results of this study with past work done by Zhuze et al. (54) on single crystal rare-earth oxides. It can be seen that the curve for the most dense Gd_2O_3 sample in this study agrees favorably with Zhuze's results.

Thermal conductivity was determined by using Equation 16 with the heat capacity data of Pankratz et al. (64) to give the data in Appendix B and Figure 10. The density was cor-

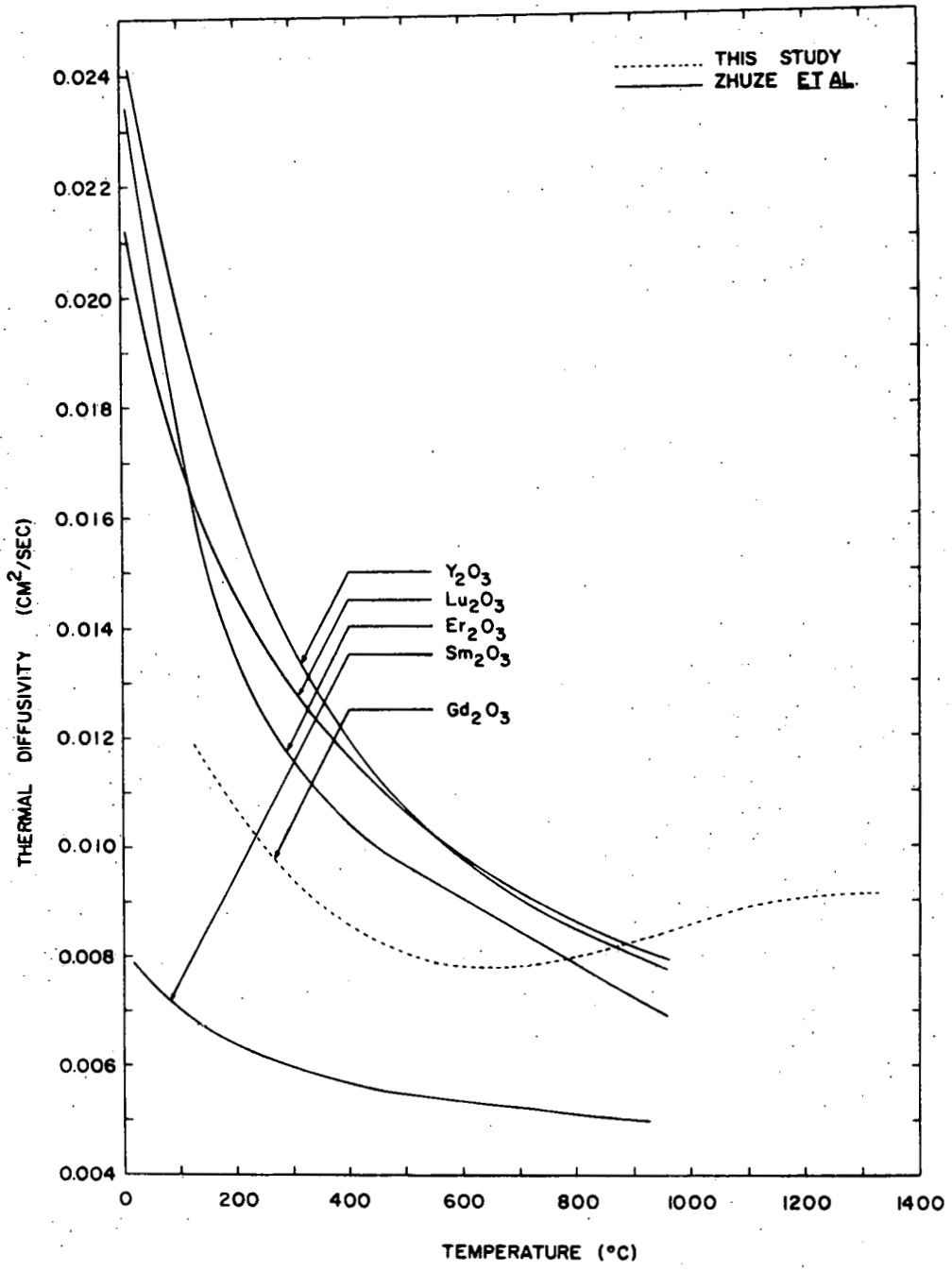

Figure 9. Thermal diffusivity versus temperature when related to past work.

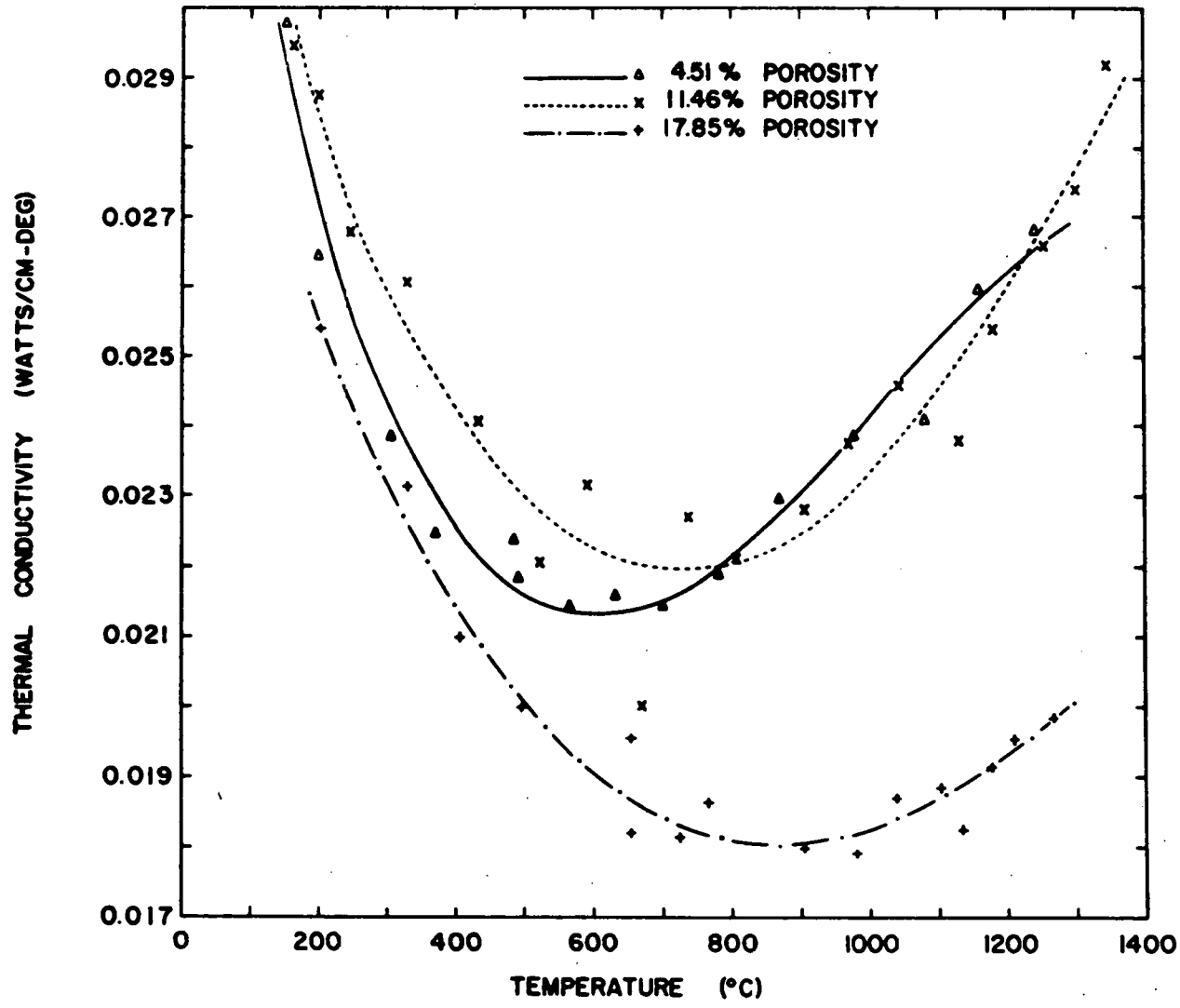

Figure 10. Thermal conductivity versus temperature.

rected for thermal expansion by the relation

$$\rho = \rho_o(1-3\alpha\Delta T) \tag{28}$$

where ρ is the density at temperature T,

ρ_o is the room temperature density,

and α and ΔT have been previously defined.

A least-squares technique was used to fit the data to an equation having the form of the resultant thermal diffusivity equations. The equations are indicated in Table VI and plotted in Figure 10.

Table VI. Equations for the temperature dependence of thermal conductivity of the form $A - BT + CT^2 - DT^3$

Volume fraction porosity	A ($\times 10^{-2}$) ($\frac{\text{watts}}{\text{cm-deg}}$)	B ($\times 10^{-5}$) ($\frac{\text{watts}}{\text{cm-deg}^2}$)	C ($\times 10^{-8}$) ($\frac{\text{watts}}{\text{cm-deg}^3}$)	D ($\times 10^{-11}$) ($\frac{\text{watts}}{\text{cm-deg}^4}$)
0.0451	5.621	9.550	8.199	2.104
0.1146	4.839	5.888	3.825	0.585
0.1785	4.254	4.891	2.944	0.472

SUMMARY AND CONCLUSIONS

The porosity dependence of Young's modulus, shear modulus, and Poisson's ratio was studied by the Forster method over the range from 2.48% to 36.78% porosity. These data were extrapolated to 0% porosity to enable calculation of the Debye temperature.

The Forster method was also used to determine the effect that temperature has on Young's and shear moduli from room temperature to 1352°C on specimens of three different porosities. It was then possible to calculate the temperature dependence of Poisson's ratio, bulk modulus, and the first (γ) and second (δ) Grüneisen constants.

Thermal diffusivity was measured over the temperature range 151-1347°C by the flash method, and the thermal conductivity was calculated from these data.

From this investigation the following conclusions can be drawn :

1. The relative Young's and shear moduli show a weaker temperature dependence than other rare-earth oxides that have been studied.
2. There is no grain boundary slippage within the temperature range of this study.
3. Higher density specimens exhibit a stronger temperature dependence for both Young's and shear moduli than less dense specimens.

4. Radiative heat transfer within material porosity was apparently a significant heat conduction mechanism above 600°C.

LITERATURE CITED

1. Ceramic Age, "Neutron-Soaking Sponges," Ceram. Age, 83 [5] 48 (1967).

2. W. C. Ziolkowski, "Austenitic Stainless Steel Alloy," Can. Pat. 803,467, Jan. 7, 1969.

3. G. Grime and J. E. Eaton, "The Determination of Young's Modulus by Flexural Vibrations," Phil. Mag., 7 [23] 96-9 (1937).

4. E. Goens, "Über Eine Dynamische Method zur Bestimmung der Temperaturabhangigkeit der Elastischen Konstanten Stabformiger Proben bei Tiefen Temperaturen," Ann. Phys., 5 [4] 733-77 (1930).

5. V. E. Giebe and E. Blechschmidt, "Über den Einfluss der Magnetisierung auf den Elastizitatsmodul bei Dehnungsschwingungen Ferromagnetischer Stabe," Ann. Phys., 5 [11] 905-36 (1931).

6. F. Forster, "Ein Neues Messverfahren zur Bestimmung des Elastizitatsmoduls und der Dampfung," Z. Metallk., 29 [4] 109-15 (1937).

7. S. Spinner and W. E. Tefft, "A Method for Determining Mechanical Resonance Frequencies and for Calculating Elastic Moduli from These Frequencies," Proc. Amer. Soc. Test. Mater., 1961, No. 61, pp. 1221-38.

8. M. O. Marlowe, "Elasticity and Kilocycle Internal Friction of Y_2O_3," M.S. Thesis, Iowa State University of Science and Technology, 1963.

9. S. Timoshenko, "On the Correction for Shear of the Differential Equation for Transverse Vibrations of Prismatic Bars," Phil. Mag., 6 [41] 744-6 (1921).

10. S. Timoshenko, "On the Transverse Vibrations of Bars of Uniform Cross-Section," Phil. Mag., 6 [43] 125-31 (1922).

11. J. W. S. Rayleigh, The Theory of Sound, 2nd ed. Dover Publications, New York, 1945.

12. A. E. H. Love, A Treatise on the Mathematical Theory of Elasticity, 4th ed. Dover Publications, New York, 1944.

13. E. Goens, "Über die Bestimmung des Elatizitatsmoduls von Staben mit Hilfe von Biegungschwingungen," Ann. Phys., 5 [11] 649-78 (1931).

14. G. Pickett, "Equations for Computing Elastic Constants from Flexural and Torsional Resonant Frequencies of Vibration of Prisms and Cylinders," Proc. Amer. Soc. Test. Mater., 1945, No. 45, pp. 846-65.

15. S. Spinner, T. W. Reichard, and W. E. Tefft, "A Comparison of Experimental and Theoretical Relations Between Young's Modulus and the Flexural and Longitudinal Resonance Frequencies of Uniform Bars," J. Res. Nat. Bur. Stand., 64A [2] 147-55 (1960).

16. J. M. Dewey, "The Elastic Constants of Materials Loaded with Non-Rigid Fillers," J. Appl. Phys., 18 [6] 578-81 (1947).

17. J. K. Mackenzie, "The Elastic Constants of a Solid Containing Spherical Holes," Proc. Phys. Soc., London, 63B [1] 2-11 (1950).

18. E. H. Kerner, "The Elastic and Thermo-Elastic Properties of Composite Media," Proc. Phys. Soc., London, 69B [8] 808-13 (1956).

19. Z. Hashin, "The Elastic Moduli of Heterogeneous Materials," J. Appl. Mech., 29 [1] 143-50 (1962).

20. R. L. Coble and D. W. Kingery, "Effect of Porosity on Physical Properties of Sintered Alumina," J. Amer. Ceram. Soc., 39 [11] 377-85 (1956).

21. M. O. Marlowe and D. R. Wilder, "Elasticity and Internal Friction of Polycrystalline Yttrium Oxide," J. Amer. Ceram. Soc., 48 [5] 227-33 (1965).

22. W. R. Manning, O. Hunter, Jr., and B. R. Powell, Jr., "Elastic Properties of Polycrystalline Yttrium Oxide, Dysprosium Oxide, Holmium Oxide, and Erbium Oxide: Room Temperature Measurements," J. Amer. Ceram. Soc., 52 [8] 436-42 (1969).

23. R. M. Spriggs, "Expression for Effect of Porosity on Elastic Modulus of Polycrystalline Refractory Materials, Particularly Aluminum Oxide," J. Amer. Ceram. Soc., 44 [12] 628-9 (1961).

24. W. Duckworth, "Discussion of Ryshkewitch Paper," J. Amer. Ceram. Soc., 36 [2] 68 (1953).

25. E. Ryshkewitch, "Compression Strength of Porous Sintered Alumina and Zirconia," J. Amer. Ceram. Soc., 36 [2] 65-8 (1953).

26. R. M. Spriggs and L. A. Brissette, "Expressions for Shear Modulus and Poisson's Ratio of Porous Refractory Oxides," J. Amer. Ceram. Soc., 45 [4] 198-9 (1962).

27. D. P. H. Hasselman, "On the Porosity Dependence of the Elastic Moduli of Polycrystalline Refractory Materials," J. Amer. Ceram. Soc., 45 [9] 452-3 (1962).

28. R. E. Fryxell and B. A. Chandler, "Creep, Strength, Expansion, and Elastic Moduli of Sintered BeO as a Function of Grain Size, Porosity, and Grain Orientation," J. Amer. Ceram. Soc., 47 [6] 283-91 (1964).

29. J. B. Wachtman, Jr., W. E. Tefft, D. G. Lam, Jr., and C. S. Apstein, "Exponential Temperature Dependence of Young's Modulus for Several Oxides," Phys. Rev., 122 [6] 1754-9 (1961).

30. W. R. Manning and O. Hunter, Jr., "Elastic Properties of Polycrystalline Yttrium Oxide, Holmium Oxide, and Erbium Oxide: High-Temperature Measurements," J. Amer. Ceram. Soc., 52 [9] 492-6 (1969).

31. H. B. Huntington, Solid State Physics, Vol. 7. Edited by F. Seitz and D. Turnbull. Academic Press, New York, 1958.

32. O. L. Anderson, "A Simplified Method for Calculating the Debye Temperature from Elastic Constants," J. Phys. Chem. Solids, 24 [7] 909-17 (1963).

33. N. Soga and O. L. Anderson, "Simplified Method for Calculating Elastic Moduli of Ceramic Powder from Compressibility and Debye Temperature Data," J. Amer. Ceram. Soc., 49 [6] 318-22 (1966).

34. O. L. Anderson, "Derivation of Wachtman's Equation for the Temperature Dependence of Elastic Moduli of Oxide Compounds," Phys. Rev., 144 [2] 553-7 (1966).

35. W. R. Manning, M. O. Marlowe, and D. R. Wilder, "Temperature and Porosity Dependence of Young's Modulus of Polycrystalline Dysprosium Oxide and Erbium Oxide," J. Amer. Ceram. Soc., 49 [4] 227-8 (1966).

36. W. R. Manning and O. Hunter, Jr., "Porosity Dependence of Young's and Shear Moduli of Polycrystalline Yttrium Oxide," J. Amer. Ceram. Soc., 51 [9] 537-8 (1968).

37. S. Spinner, F. P. Knudsen, and L. Stone, "Elastic Constant - Porosity Relations for Polycrystalline Thoria," J. Res. Nat. Bur. Stand., 67C [1] 39-46 (1963).

38. S. Spinner, L. Stone, and F. P. Knudsen, "Temperature Dependence of the Elastic Constants of Thoria Specimens of Varying Porosity," J. Res. Nat. Bur. Stand., 67C [2] 93-100 (1963).

39. B. R. Powell, Jr., O. Hunter, Jr., and W. R. Manning, "Elastic Properties of Polycrystalline Ytterbium Oxide," J. Amer. Ceram. Soc., 54 [10] 488-90 (1971).

40. W. R. Manning and O. Hunter, Jr., "Elastic Properties of Polycrystalline Thulium Oxide and Lutetium Oxide from 20° to 1000°C," J. Amer. Ceram. Soc., 53 [5] 279-80 (1970).

41. A. J. Angstron, "Neue Methods, das Warmeleitungsuermogen der Koper zu Bestimmen," Ann. Phys. und Chem., 114, 513-30 (1861).

42. W. J. Parker, R. J. Jenkins, C. P. Butler, and G. L. Abbott, "Flash Method of Determining Thermal Diffusivity, Heat Capacity, and Thermal Conductivity," J. Appl. Phys., 32 [9] 1679-84 (1961).

43. T. M. Branscomb, "Thermal Diffusivity of TiB_2, ZrB_2, and HfB_2," M.S. Thesis, Iowa State University of Science and Technology, 1970.

44. T. M. Branscomb and O. Hunter, Jr., "Improved Thermal Diffusivity Method Applied to TiB_2, ZrB_2, and HfB_2 from 200°-1300°C," J. Appl. Phys., 42 [6] 2309-15 (1971).

45. B. H. Morrison, D. J. Klein, and L. R. Cowder, "Thermal Diffusivity of Pyrolytic Graphite from 25 to 1900°C," U.S. At. Energy Comm. LA-DC-8307, Los Alamos Scientific Lab., University of California, Los Alamos, New Mexico, 1967.

46. R. Iacobelli and S. Moretti, "Thermal Diffusivity and Conductivity Measurements on Metals and Oxides at High Temperatures," Rev. Hautes Temper. et Refract., 3 [2] 215-28 (1966).

47. J. B. Moser and O. L. Kruger, "Heat Pulse Measurements on Uranium Compounds," J. Nucl. Mater., 17 [2] 153-8 (1965).

48. H. W. Deem and W. D. Wood, "Flash Thermal Diffusivity Measurements Using a Laser," Rev. Sci. Inst., 33 [10] 1107-9 (1962).

49. D. E. Baker, "Thermal Conductivity of Irradiated Graphite by a Rapid Thermal Pulse Method," J. Nucl. Mater., 12 [1] 120-4 (1964).

50. R. J. Freeman, "Thermal Diffusivity of Pre- and Post-Irradiated BeO," U.S. At. Energy Comm. GEMP-452, General Electric Company Flight Propulsion Lab., Cincinnati, Ohio, 1966.

51. D. Shaw and L. A. Goldsmith, "An Apparatus to Measure the Thermal Diffusivity of Irradiated Fuel Specimens at Temperatures up to 1200°C by the Flash Method," J. Sci. Inst., 43 [8] 594-6 (1966).

52. M. Murabayashi, S. Namba, Y. Takahashi, and T. Mukaibo, "Thermal Conductivity of ThO_2-UO_2 System," J. Nucl. Sci. and Tech., 6 [3] 128-31 (1969).

53. J. B. Moser and O. L. Kruger, "Thermal Conductivity and Heat Capacity of the Monocarbide, Monophosphide, and Monosulfide of Uranium," J. Appl. Phys., 38 [8] 3215-22 (1967).

54. V. P. Zhuze, O. N. Novruzov, A. A. Popova, and A. I. Shelykh, "Thermal Diffusivities of Y_2O_3, Er_2O_3, Lu_2O_3, and Sm_2O_3 Single Crystals," Izv. Akad. Nauk SSSR, Neorg. Mater., 4 [9] 1493-7 (1968).

55. B. H. Morrison, "Thermal Diffusivity of ATJ-S Graphite from 100° to 3000°K," Los Alamos Scientific Lab., University of California, Los Alamos, New Mexico; unpublished.

56. M. M. Nakata, R. A. Finch, and C. J. Ambrose, "Thermophysical Properties of Zirconium-Uranium Hydrides," Proc. Therm. Cond., 1966, No. 6, pp. 479-507.

57. C. C. Weeks, M. M. Nakata, and C. A. Smith, "Thermal Properties of SNAP Fuels," Proc. Therm. Cond., 1967, No. 7, pp. 387-98.

58. S. Stecura, "Crystallographic Modifications and Kinetics of Phase Transformations of La_2O_3, Nd_2O_3, Sm_2O_3, Eu_2O_3, and Gd_2O_3," Ph.D. Thesis, Georgetown University, 1965.

59. D. P. H. Hasselman, "Tables for the Computation of Shear Modulus and Young's Modulus of Elasticity from Resonant Frequencies of Rectangular Prisms," Carborundum Co., Niagara Falls, New York, 1961.

60. D. W. Stacy, "Thermal Expansion of the Sesquioxides of Yttrium, Scandium, and Gadolinium," M.S. Thesis, Iowa State University of Science and Technology, 1967.

61. B. Schwartz, "Thermal Stress Failure of Pure Refractory Oxides," J. Amer. Ceram. Soc., 35 [12] 325-33 (1952).

62. J. B. Wachtman, Jr. and D. G. Lam, Jr., "Young's Modulus of Various Refractory Materials as a Function of Temperature," J. Amer. Ceram. Soc., 42 [5] 254-60 (1959).

63. S. Spinner, "Temperature Dependence of Elastic Constants of Some Cermet Specimens," J. Res. Nat. Bur. Stand., 65C [2] 89-96 (1961).

64. L. B. Pankratz, E. G. King, and K. K. Kelley, "High-Temperature Heat Contents and Entropies of Sesquioxides of Europium, Gadolinium, Neodymium, Samarium, and Yttrium," U.S. Bur. Mines, No. 6033, pp. 7-9 (1962).

65. J. J. Martin, P. H. Sidles, and G. C. Danielson, "Thermal Diffusivity of Platinum from 300° to 1200°K," J. Appl. Phys., 38 [8] 3075-8 (1967).

66. J. C. VanCraeynest, J. C. Weilbacher, and J. C. Salbreux, "Thermal Conductivity of Mixed Uranium and Plutonium Carbides, Nitrides, and Carbonitrides," presented at Centre d'Etudes Nucleaires de Fontenay-aux-Roses, France, Oct. 1968.

67. D. R. Flynn, "Thermal Conductivity of Ceramics," Nat. Bur. Stand., No. 303, pp. 78-81 (1968).

APPENDIX A. ELASTICITY DATA

Table AI. Dimensions, densities, and volume fraction porosities of resonant frequency specimens

Specimen no.	Length (cm)	Width (cm)	Thickness (cm)	Density (g/cm^3)	Volume fraction porosity
2-2 A	6.922	0.652	0.246	6.470	0.2251
2-2 B	7.432	0.740	0.317	6.444	0.2282
2-2 C	7.404	0.730	0.298	6.444	0.2282
2-2 D	7.323	0.803	0.234	6.428	0.2297
3-3 A	7.328	0.718	0.301	5.342	0.3599
3-3 B	7.805	0.614	0.301	5.359	0.3582
3-3 D	7.716	0.718	0.258	5.426	0.3497
4-4 A	7.939	0.849	0.356	5.276	0.3678
4-4 B	7.963	0.830	0.396	5.301	0.3651
4-4 C	7.955	0.845	0.323	5.326	0.3617
4-4 D	7.935	0.774	0.289	5.292	0.3660
5-5 A	6.045	0.488	0.180	7.454	0.1072
5-5 B	6.241	0.466	0.212	7.296	0.1256
5-5 D	5.558	0.496	0.153	7.371	0.1174
6-6 A	5.450	0.536	0.128	8.056	0.0347
6-8 A	5.057	0.537	0.147	8.114	0.0280
6-9 A	4.685	0.570	0.170	8.139	0.0248
7-6 A	4.120	0.719	0.212	6.603	0.2086

Table A II. Room temperature resonant frequencies and elastic properties

Specimen no.	Volume fraction porosity	Flexural resonant frequency (hertz)	Torsional resonant frequency (hertz)	Young's modulus (kilobars)	Shear modulus (kilobars)	Poisson's ratio
2-2 A	0.2251	1962.45	10,385.65	903.92	352.21	0.2832
2-2 B	0.2282	2176.55	4,958.45	892.07	345.82	0.2898
2-2 C	0.2282	2072.65	4,954.75	898.88	348.50	0.2896
2-2 D	0.2297	1665.35	5,507.40	892.53	347.11	0.2856
3-3 A	0.3599	1849.20	4,320.80	559.87	220.38	0.2702
3-3 B	0.3582	1633.95	3,281.00	559.37	221.22	0.2692
3-3 D	0.3497	1464.70	3,941.60	586.37	231.28	0.2676
4-4 A	0.3678	1843.65	4,273.30	541.97	213.83	0.2672
4-4 B	0.3651	2034.50	4,138.70	540.89	215.10	0.2573
4-4 C	0.3617	1686.40	4,237.30	551.46	219.47	0.2564
4-4 D	0.3660	1494.10	3,904.95	538.52	213.37	0.2620
5-5 A	0.1072	2038.60	5,415.35	1211.55	473.40	0.2796
5-5 B	0.1256	2231.40	4,796.25	1160.08	459.90	0.2612
5-5 D	0.1174	2013.50	6,422.65	1166.82	456.45	0.2782
6-6 A	0.0347	1855.10	7,527.60	1414.18	557.82	0.2676
6-8 A	0.0280	2482.55	8,728.90	1434.55	569.45	0.2596
6-9 A	0.0248	3384.50	10,793.60	1479.00	574.84	0.2864
7-6 A	0.2086	4731.10	14,863.80	925.37	354.25	0.3061

Table A III. Elevated temperature resonant frequencies and elastic properties for specimen 4-4 D having 36.60% porosity

Temp. (°C)	Flexural resonant frequency (hertz)	Torsional resonant frequency (hertz)	Young's modulus (kilobars)	Shear modulus (kilobars)	Poisson's ratio	Bulk modulus (kilobars)
48	1487.10	7680.95	535.99	212.16	0.2632	377.20
82	1479.40	7642.60	530.28	209.98	0.2627	372.43
138	1470.45	7595.35	523.60	207.28	0.2630	368.25
177	1466.35	7569.65	520.50	205.80	0.2646	368.49
240	1457.80	7519.35	514.14	202.95	0.2666	367.24
310	1448.25	7473.90	507.08	200.37	0.2653	360.18
383	1439.35	7425.60	500.52	197.66	0.2662	356.67
452	1429.75	7379.25	493.55	195.07	0.2651	350.12
506	1422.05	7336.00	488.00	192.69	0.2663	348.00
560	1415.10	7305.20	482.99	190.98	0.2645	341.82
633	1405.50	7254.35	476.13	188.20	0.2650	337.62
681	1399.75	7224.80	472.02	186.58	0.2649	334.85
743	1391.90	7189.40	466.47	184.65	0.2631	328.20
796	1385.15	7162.75	461.73	183.19	0.2602	320.98
846	1377.45	7106.65	456.39	180.25	0.2660	325.05
898	1370.05	7072.15	451.28	178.41	0.2647	319.68
956	1362.25	7033.70	445.91	176.38	0.2640	314.99
1010	1355.45	6997.30	441.24	174.47	0.2645	312.29
1052	1349.50	6964.70	437.21	172.78	0.2652	310.37
1102	1342.60	6931.70	432.54	171.07	0.2642	304.80
1144	1337.30	6902.30	428.96	169.55	0.2650	304.22
1182	1332.55	6878.05	425.77	168.30	0.2649	301.85
1222	1326.90	6845.05	422.01	166.63	0.2663	300.97
1271	1320.00	6811.50	417.44	164.92	0.2656	296.79
1305	1315.25	6781.75	414.31	163.43	0.2675	297.05
1347	1307.90	6745.80	409.53	161.64	0.2668	292.68

Table A IV. Elevated temperature resonant frequencies and elastic properties for specimen 2-2 D having 22.97% porosity

Temp. (°C)	Flexural resonant frequency (hertz)	Torsional resonant frequency (hertz)	Young's modulus (kilobars)	Shear modulus (kilobars)	Poisson's ratio	Bulk modulus (kilobars)
58	1654.88	7921.50	883.16	341.65	0.2925	709.34
104	1646.50	7829.00	873.95	333.57	0.3100	766.60
156	1638.05	7815.05	864.57	332.22	0.3012	724.83
199	1632.50	7816.55	858.37	332.21	0.2919	687.49
258	1624.20	7762.20	849.19	327.42	0.2968	696.48
331	1613.55	7731.60	837.51	324.62	0.2900	671.90
392	1605.75	7704.85	828.95	322.19	0.2864	646.90
456	1596.55	7639.05	818.98	316.52	0.2937	661.72
523	1587.35	7593.95	809.05	312.60	0.2941	654.78
565	1581.60	7563.10	802.88	309.94	0.2952	653.44
641	1570.30	7517.30	790.88	305.98	0.2924	634.85
692	1564.05	7488.50	784.22	303.49	0.2920	628.39
742	1557.20	7451.20	776.99	300.33	0.2936	627.29
800	1549.55	7424.35	768.96	298.01	0.2902	610.74
845	1542.20	7393.20	761.36	295.39	0.2888	600.64
911	1532.40	7341.70	751.24	291.10	0.2903	597.21
963	1525.50	7308.50	744.13	288.33	0.2904	591.74
1010	1518.10	7276.20	736.60	285.66	0.2893	582.65
1056	1512.00	7245.70	730.37	283.15	0.2897	578.89
1101	1505.60	7215.15	723.90	280.65	0.2897	573.66
1145	1498.70	7180.35	716.98	277.83	0.2903	569.90
1181	1493.10	7146.05	711.39	275.09	0.2930	572.81
1218	1487.75	7122.05	706.06	273.15	0.2924	566.95
1271	1478.60	7080.30	697.04	269.82	0.2917	557.66
1308	1472.65	7051.30	691.21	267.53	0.2918	553.42
1351	1464.20	7008.30	683.02	264.16	0.2928	549.44

Table A V. Elevated temperature resonant frequencies and elastic properties for specimen 6-6 A having 3.47% porosity

Temp. (°C)	Flexural resonant frequency (hertz)	Torsional resonant frequency (hertz)	Young's modulus (kbars)	Shear modulus (kbars)	Poisson's ratio	Bulk modulus (kbars)	Grüneisen constants γ	Grüneisen constants δ
51	1851.35	10,352.70	1403.66	553.29	0.2685	1010.41	1.1946	2.5309
96	1846.40	10,324.30	1395.41	550.02	0.2685	1004.65	1.1576	2.9171
144	1845.35	10,322.15	1393.34	549.54	0.2677	999.81	1.1293	3.2400
185	1839.90	10,296.35	1384.58	546.58	0.2666	988.64	1.1020	3.4884
255	1833.55	10,255.80	1374.12	541.92	0.2678	986.41	1.0804	3.7748
317	1826.10	10,205.45	1362.19	536.30	0.2700	987.05	1.0678	3.9560
381	1818.50	10,167.05	1350.05	531.95	0.2690	973.91	1.0423	4.1579
450	1812.30	10,137.25	1339.98	528.49	0.2677	961.57	1.0187	4.3376
511	1807.90	10,101.70	1332.70	524.48	0.2705	967.81	1.0171	4.3979
566	1799.65	10,063.05	1319.89	520.21	0.2686	950.71	0.9925	4.5429
635	1793.45	10,027.80	1309.95	516.23	0.2688	944.17	0.9778	4.6455
688	1787.10	9,990.30	1300.04	512.12	0.2692	939.09	0.9669	4.7159
742	1779.50	9,950.90	1288.34	507.83	0.2685	927.43	0.9495	4.8155
800	1772.60	9,908.95	1277.67	503.28	0.2693	923.21	0.9396	4.8750
874	1765.55	9,866.70	1266.64	498.65	0.2701	918.13	0.9277	4.9429
902	1761.40	9,847.65	1260.36	496.60	0.2690	909.31	0.9163	5.0046
952	1755.20	9,813.05	1250.91	492.88	0.2690	902.46	0.9051	5.0653
1010	1751.10	9,791.70	1244.39	490.47	0.2686	896.16	0.8940	5.1244
1053	1745.35	9,760.45	1235.73	487.14	0.2683	889.09	0.8835	5.1810
1107	1738.85	9,722.70	1225.92	483.14	0.2687	883.36	0.8735	5.2326
1159	1734.45	9,700.60	1219.12	480.71	0.2680	875.96	0.8623	5.2925
1190	1728.20	9,662.10	1210.00	476.76	0.2690	872.95	0.8570	5.3194
1226	1726.15	9,658.30	1206.72	476.22	0.2670	863.09	0.8446	5.3900
1274	1721.75	9,629.70	1200.03	473.19	0.2680	862.17	0.8403	5.4073
1318	1713.25	9,579.40	1187.73	468.07	0.2687	856.03	0.8312	5.4561
1353	1708.00	9,550.45	1180.07	465.09	0.2686	850.12	0.8231	5.5015

APPENDIX B. THERMAL DIFFUSIVITY DATA

Table B I. Thicknesses, densities, and volume fraction porosities of thermal diffusivity specimens

Sample no.	Thickness (cm)	Density (g/cm^3)	Volume fraction porosity
TD-3	0.160	6.857	0.1785
Gd-4	0.169	7.391	0.1146
Gd-13	0.159	7.971	0.0451

Table B II. Elevated temperature times, thicknesses, thermal diffusivities and conductivities for specimen TD-3 having 17.85% porosity

Temp. (°C)	L (cm)	$t_{1/2}$ (sec)			α_T (cm^2/sec)				λ (watts/cm-deg)
		1	2	3	1	2	3	avg	
203	0.160230	0.297	0.320	0.307	0.01201	0.01115	0.01162	0.01158	0.02539
330	0.160410	0.350	0.338	0.358	0.01022	0.01058	0.00999	0.01026	0.02313
406	0.160521	0.380	0.380	0.405	0.00942	0.00942	0.00884	0.00922	0.02100
495	0.160653	0.413	0.423	0.407	0.00868	0.00848	0.00881	0.00866	0.02000
652	0.160893	0.438	0.435	0.423	0.00819	0.00825	0.00848	0.00831	0.01955
723	0.161004	0.470	0.490	0.450	0.00763	0.00735	0.00801	0.00766	0.01816
763	0.161068	0.485	0.450	0.445	0.00743	0.00801	0.00810	0.00784	0.01866
902	0.161293	0.472	0.505	0.478	0.00766	0.00716	0.00756	0.00746	0.01800
978	0.161419	0.525	0.453	0.495	0.00690	0.00799	0.00732	0.00737	0.01791
1038	0.161520	0.468	0.478	0.475	0.00775	0.00758	0.00763	0.00766	0.01871
1102	0.161627	0.480	0.470	0.470	0.00756	0.00772	0.00772	0.00766	0.01887
1134	0.161684	0.525	0.455	0.490	0.00692	0.00798	0.00741	0.00741	0.01826
1176	0.161756	0.480	0.477	0.450	0.00758	0.00762	0.00808	0.00775	0.01916
1210	0.161815	0.475	0.445	0.460	0.00766	0.00818	0.00789	0.00789	0.01956
1265	0.161912	0.465	0.457	0.450	0.00783	0.00797	0.00810	0.00797	0.01985

Table B III. Elevated temperature times, thicknesses, thermal diffusivities and conductivities for specimen Gd-4 having 11.46% porosity

Temp. (°C)	L (cm)	$t_{1/2}$ (sec)			α_T (cm^2/sec)				λ (watts/cm-deg)
		1	2	3	1	2	3	avg	
161	0.169180	0.315	0.325	0.306	0.01263	0.01224	0.01300	0.01262	0.02947
200	0.169238	0.330	0.340	0.310	0.01206	0.01171	0.01284	0.01218	0.02877
247	0.169308	0.357	0.357	0.353	0.01116	0.01116	0.01127	0.01120	0.02677
330	0.169433	0.380	0.374	0.360	0.01050	0.01067	0.01108	0.01074	0.02609
432	0.169590	0.410	0.415	0.408	0.00975	0.00963	0.00980	0.00973	0.02402
523	0.169734	0.443	0.473	0.437	0.00904	0.00846	0.00916	0.00883	0.02206
592	0.169845	0.436	0.446	0.425	0.00919	0.00899	0.00943	0.00920	0.02318
670	0.169973	0.490	0.515	0.515	0.00819	0.00780	0.00780	0.00792	0.02006
737	0.170084	0.440	0.475	0.445	0.00914	0.00846	0.00903	0.00871	0.02270
807	0.170202	0.480	0.453	0.475	0.00839	0.00889	0.00848	0.00858	0.02211
907	0.170374	0.455	0.475	0.450	0.00886	0.00849	0.00896	0.00877	0.02282
970	0.170484	0.440	0.455	0.440	0.00918	0.00888	0.00918	0.00908	0.02376
1044	0.170615	0.430	0.443	0.428	0.00941	0.00913	0.00945	0.00933	0.02458
1131	0.170772	0.440	0.425	0.450	0.00921	0.00954	0.00901	0.00925	0.02379
1187	0.170875	0.420	0.425	0.433	0.00966	0.00955	0.00937	0.00952	0.02539
1255	0.170999	0.410	0.403	0.417	0.00991	0.01008	0.00974	0.00991	0.02659
1302	0.171089	0.420	0.390	0.390	0.00968	0.01043	0.01043	0.01017	0.02739
1347	0.171173	0.365	0.380	0.385	0.01116	0.01072	0.01058	0.01081	0.02922

Table B IV. Elevated temperature times, thicknesses, thermal diffusivities and conductivities for specimen Gd-13 having 4.51% porosity

Temp. (°C)	L (cm)	$t_{1/2}$ (sec)			α_T (cm^2/sec)				λ (watts/cm-deg)
		1	2	3	1	2	3	avg	
151	0.159156	0.290	0.295	0.305	0.01214	0.01193	0.01154	0.01187	0.02979
199	0.159223	0.347	0.335	0.337	0.01015	0.01052	0.01045	0.01038	0.02644
304	0.159370	0.377	0.385	0.395	0.00936	0.00917	0.00894	0.00915	0.02386
371	0.159467	0.408	0.416	0.420	0.00866	0.00850	0.00841	0.00852	0.02248
486	0.159635	0.425	0.425	0.423	0.00833	0.00833	0.00837	0.00835	0.02240
492	0.159645	0.433	0.440	0.433	0.00818	0.00805	0.00818	0.00814	0.02185
564	0.159753	0.448	0.455	0.440	0.00792	0.00780	0.00806	0.00792	0.02145
631	0.159855	0.440	0.450	0.454	0.00807	0.00789	0.00782	0.00793	0.02164
698	0.159958	0.453	0.455	0.460	0.00785	0.00782	0.00773	0.00780	0.02144
782	0.160091	0.445	0.457	0.450	0.00800	0.00779	0.00792	0.00790	0.02190
870	0.160233	0.437	0.430	0.437	0.00816	0.00830	0.00816	0.00822	0.02298
978	0.160410	0.430	0.425	0.415	0.00832	0.00841	0.00862	0.00845	0.02387
1081	0.160582	0.427	0.430	0.416	0.00837	0.00833	0.00862	0.00845	0.02409
1161	0.160719	0.403	0.397	0.390	0.00891	0.00904	0.00920	0.00905	0.02598
1242	0.160860	0.395	0.388	0.380	0.00910	0.00927	0.00946	0.00928	0.02682

ACKNOWLEDGEMENTS

The author would like to express his sincere gratitude to Dr. O. Hunter, Jr. for his guidance and encouragement throughout the course of this research, to Dr. M. O. Marlowe for building the original sonic resonance equipment, to Mr. T. M. Branscomb for building the thermal diffusivity equipment, to Mr. F. W. Calderwood for his assistance in the thermal diffusivity measurements, to Miss Verna Thompson for typing this thesis, and to his wife, Sharon, for her patience and understanding.